Measurements and Modeling of Distributed Antenna Systems in Railway Tunnels

Cesar Briso-Rodríguez, Javier M. Cruz, and Jose I. Alonso, *Member, IEEE*

***Abstract*—This paper covers some of the work carried out in the planning of the Global System for Mobile Communication for Railway (GSM-R) of the tunnels on the new high-speed trains in Spain. Solutions based on distributed antenna systems have been tested by installing several 900-MHz transmitters inside and outside of a 4000-m tunnel and measuring the propagation in different conditions. The measurements have been used to model the effects of tunnel propagation, including curves, trains passing from the outside to the inside, and the effect of two trains passing inside the tunnel. All cases have been tested by comparing solutions using isofrequency and multifrequency distributed transmitters inside the tunnel. The improvements of signal-to-noise ratio and the reduction of the blocking effects of two trains passing have demonstrated the advantages of using isofrequency distributed antenna systems in tunnels. Finally, a complete propagation model combining both modal analysis and ray tracing has been applied to predict the propagation loss inside and outside these tunnels, and results have been compared with the measurements. The model has proven to be very useful for radio planning in new railway networks.**

***Index Terms*—Distributed antenna, Global System for Mobile Communication for Railway (GSM-R), modal analysis, propagation in tunnels.**

I. Introduction

TRADITIONALLY, radio coverage inside the tunnels for railway trains is usually achieved using leaky feeders. This technique does not require special planning, and a good coverage in all types of tunnel is obtained. Nevertheless, the main disadvantages of leaky feeders are high cost, maintenance, and installation difficulties. These problems are easily solved in short tunnels, but new high-speed trains frequently require medium or long tunnels, and in this case, the leaky feeder solution becomes too expensive. For these reasons, solutions that are based on the use of antennas are becoming more interesting.

Radio coverage with antennas requires an accurate prediction of propagation loss inside and outside the tunnel, particularly when the communication system must maintain a high quality of service along the entire track [1]–[4]. New European high-speed trains have adopted a Global System for Mobile Communication (GSM)-based communication system for data and voice communications, which is called GSM Railway (GSM-R) [5], [6]. This system has a proprietary frequency band (876–880 MHz uplink and 921–925 MHz downlink), and the network must have a very high quality of service because it is used for the signaling and control of the trains. This paper presents measurements that are taken in one of the longest tunnels of the new 450-km high-speed train line from Madrid to Lleida in Spain. The measurements have been applied to develop a propagation model for railway tunnel coverage that is based on the use of distributed antennas. The model uses modal analysis combined with ray tracing to predict the propagation attenuation inside the tunnel.

II. Measurements

Propagation prediction and modeling of radio coverage inside a tunnel depend on the section, curves, and construction characteristics of the walls. Several reports on measurements have been published [7]–[10], but there are important differences between tunnels for cars or trains, as well as in the railway environment between subway, light trains, or high-speed trains.

Railway tunnels have special characteristics: ballast on the ground, variable semicircular section, overhead cables, construction in concrete, smooth curves, etc. On a high-speed train line, there are usually several tunnels with lengths ranging from several hundred meters to several kilometers, and these tunnels are part of a cellular network, so that a handover must be made in some part of the tunnel: at the entrance, in the middle, or at the exit. Therefore, the objective of the measurements was to model radio coverage inside and outside the tunnel to determine the optimum distance between repeaters, the number of repeaters required, handover points, and signal margins. It was also necessary to test new solutions based on the use of isofrequency repeaters and directional antennas and the influence of trains passing inside the tunnel. The final objective was to get high-quality communications inside long tunnels using distributed antenna systems.

Manuscript received January 27, 2005; revised May 17, 2006, November 2, 2006, and January 16, 2007. This work was supported in part by the Spanish high-speed railway infrastructure operator (GIF) and in part by the National Board of Scientific and Technology Research (Comisión Interministerial de Ciencia y Tecnología) under Project TEC 2005-07010-C02-01/TCM. The review of this paper was coordinated by Prof. D. Michelson.

C. Briso-Rodríguez is with the Departamento de Ingeniería Audiovisual y Comunicaciones, Escuela Universitaria de Ingeniería Técnica de Telecomunicación, Universidad Politécnica de Madrid, 28031 Madrid, Spain (e-mail: cbriso@diac.upm.es).

J. M. Cruz is with the Metropolian of Tenerife, Santa Cruz de Tenerife, 38003 Spain.

J. I. Alonso is with the Departamento de Señales, Sistemas y Radiocomunicaciones, Escuela Técnica Superior de Ingenieros de Telecomunicación, Universidad Politecnica de Madrid, 28040 Madrid, Spain (e-mail: ignacio@gmr.ssr.upm.es).

Color version of one or more of the figures in the paper are available online at http://ieeexplore.ieee.org.

Digital Object Identifier 10.1109/TVT.2007.900500

Fig. 1. Tunnel and train used in the measurements.

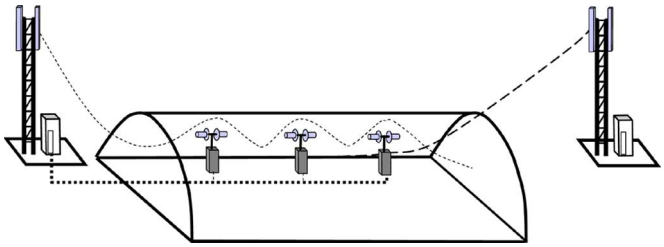

Fig. 2. Configuration of repeaters and BTSs.

A. Environment and Measurement System

The tunnel measured has a total length of 4000 m with a smooth curve in the middle. The section is arched, with a circular shape of radius $R = 6.2$ m and floor width $a = 10.7$ m. Fig. 1 shows a photograph of the tunnel.

The objective of the trial was to evaluate the radio coverage throughout the tunnel; for this purpose, an initial estimation suggested that four transmitters were needed. This estimation was based on the modal analysis propagation model that was used and on the minimum signal level that was specified by the GSM-R system, which is -70 dBm inside the tunnel and -85 dBm outside.

The final configuration can be implemented using repeaters and base stations. Fig. 2 shows this configuration with one GSM-R base transmitter station (BTS) at the entrance with three repeaters connected to it and another BTS at the output of the tunnel. Because of the length of the tunnel, the repeaters use "radio over fiber technology." This technology permits the electrical 900-MHz signal of the BTS to be converted to optical and transmit it to and receive it from the repeaters through a monomode fiber optic. In the repeaters, the signal is converted again into an electrical signal amplified and transmitted/received. This configuration permits a maximum separation of 20 km from the BTS to the repeaters. In the tunnel, each repeater has two high gain antennas: one pointing to each side of the tunnel to achieve overlapping of the coverage, and at the exit of the tunnel, where there is a second BTS with an antenna pointing into the tunnel. At this point, the trains make a handover to the second BTS. As the output signal of the BTS is converted (i.e., electrical–optical–electrical), the output frequency of the repeaters is coherent with the frequency of the BTS inside the coherence bandwidth of the GSM-R channels (200 kHz).

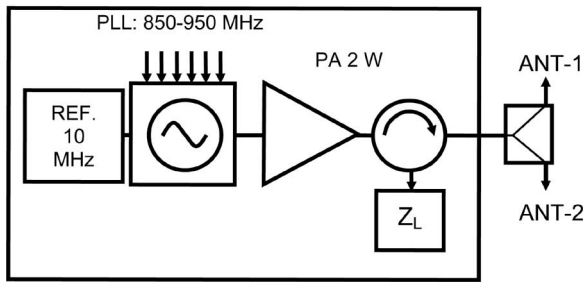

Fig. 3. Test transmitter.

To test the tunnel, four 900-MHz transmitters were used. Three transmitters were located inside the tunnel to emulate the repeaters at 1000, 2300, and 3500 m with two antennas: one pointing to each side of the tunnel. The fourth transmitter was located 2000 m from the other entrance with a line-of-sight propagation to the tunnel entrance to emulate the external GSM-R BTS. The external transmitter has only one antenna pointing to the entrance of the tunnel. The first BTS was not emulated to simplify measurements.

The transmitters used are proprietary portable equipment (see Fig. 3) that covers the 900-MHz GSM-R band in 200-kHz steps with an output power of 2 W. Each transmitter has a frequency synthesizer and a high-stability 10-MHz reference that provides a high-output frequency accuracy. The transmitters are small and can be powered with a 12-V battery. In the measurements, the output signal of each transmitter inside the tunnel was divided with a 3-dB power splitter to feed two antennas, with one pointing to each extreme of the tunnel. The entire equipment was individually calibrated using a power meter.

The antenna used in all transmitters was a 15-dBi gain helical antenna with 60° E and H main lobe, circular polarization, and 20-dB front-to-back ratio. Inside the tunnel, the antennas were located on a 4-m mast 20 cm from the tunnel walls. Outside the tunnel, at the north entrance, another transmitter was installed to emulate the future location of a GSM-R BTS. This transmitter has 2 W of power and uses only one 15-dB gain helical antenna pointing to the entrance of the tunnel. There was a line of sight from the location of the transmitter to the north entrance of the tunnel.

Two trains were used for the measurements, one was the mobile station and the other was used to reproduce blocking effects inside the tunnel. The trains have three carriages, 60 m

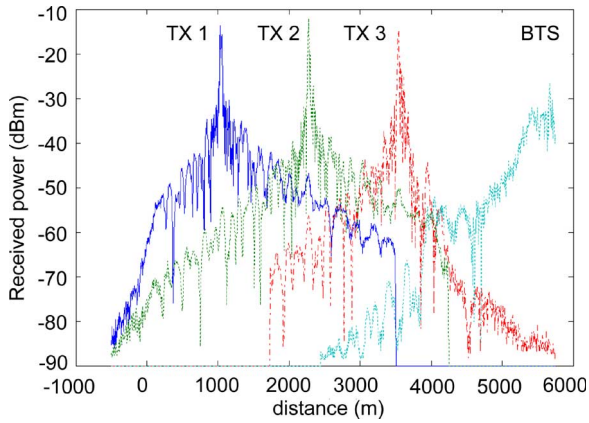

Fig. 4. Coverage of tunnels with multifrequency transmitters. Tunnel from 0 to 4000 m.

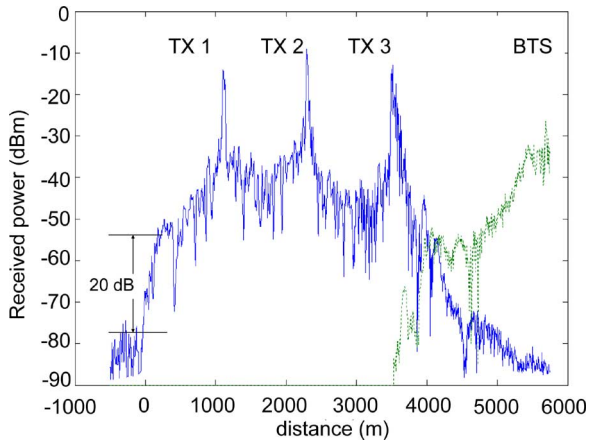

Fig. 5. Coverage of tunnels with three isofrequency transmitters inside the tunnel and one transmitter outside. Tunnel from 0 to 4000 m.

in length. The measurement equipment deployed in the locomotive cabin of one of the trains was made up of a spectrum analyzer, a portable computer, a control software, and an external antenna. The receiving antenna was a $\lambda/4$ vertical monopole with a 2.15-dBi gain installed on the top of a train locomotive. This test system was able to take one measurement every 60 ms. Speed and position were also recorded with an electronic odometer that was installed in the train to maintain a constant measuring speed.

B. Measurements Results

Measurements were taken with the transmitters in two configurations: 1) multifrequency and 2) isofrequency.

In the first case, all the transmitters had different frequencies. This configuration was used to analyze the individual responses of the tunnel, homogeneity, and influence of curves and to compare with the improvements that were obtained with the use of isofrequency transmitters. This measurement also reproduces the coverage of the tunnel with GSM-R base stations and therefore permits the possibility of making handovers in between two transmitters to be analyzed inside the tunnel. This solution can be used in long tunnels or in any case when it is necessary to make a handover inside the tunnel. Fig. 4 shows the root-mean-square (rms) power level in the entire tunnel for multifrequency transmitters.

The second test trial uses the same frequency (isofrequency) for the three transmitters that are located inside the tunnel and different frequencies for the external transmitter. This configuration reproduces the coverage of the tunnel with the scheme of Fig. 2 without the first BTS. Results of this configuration are shown in Fig. 5.

Both graphs show how the signal reached high levels in the proximity of the repeaters and decreased very quickly at 200–300 m from it. After that, the propagation loss is much slower. This phenomenon is due to multimode propagation close to the source and to monomode when it is far from the source. The separation of these two regions can be computed, as described in [17].

Another interesting fact is the moderate signal decay when the train passes from inside to outside the tunnel. We have detailed the value measured in Fig. 5 on one side of the tunnel. We considered that this fading is caused by the wave impedance change and diffraction effects in the edge of the tunnel, and it depends mainly on the tunnel section. The signal transmitted at the edges of the tunnel is attenuated 15–20 dB when it passes from inside to outside or from outside to inside. This effect is observed mainly in the transmission coefficient because the reflected wave is rapidly attenuated; nevertheless, we can also appreciate in Fig. 5 moderate signal fluctuations on both sides of the tunnel. The result is important for network planning because it affects the location of the first and last repeaters inside the tunnel and the transmitter outside it. We can find a detailed model based on a ray-tracing technique that is described in [20].

Another of the objectives of the measurements was to test the benefits of using isofrequency transmitters with several antennas (multiple-input–multiple-output techniques) and simulcast transmission inside the tunnels. On a real network, the tunnel will have three repeaters, each one with two antennas and all connected to a GSM-R base station. With this configuration, the repeaters transmit the same information at the same frequency; therefore, the receiver located in between two repeaters receives two signals with equal frequency and without phase coherence. In this configuration, as there is no phase coherence, the received power is the power sum of signals received in the coherence bandwidth of the receiver. Therefore, if the coverage of the tunnels is designed correctly, there is an important quality of signal improvements in the central region between two repeaters. To evaluate the real signal improvement, first, we have represented the fast variations of the received signal throughout the tunnel for multifrequency transmitters, as detailed in Fig. 6. This measurement is computed as the difference between the samples recorded, i.e., $y'[n] = y[n] - y[n-1]$, and represents the fast variations of the signal. To process these data using different frequency transmitters, we have considered that the receiver is always taking the best received signal, therefore making a handover when the signal of a new transmitter is higher than the signal of the precedent transmitter. In Fig. 6, we can see that the standard deviation of the fast signal variations for multifrequency transmitters is $\sigma = 4.9$ dB, whereas the same measurement for isofrequency transmitters has a

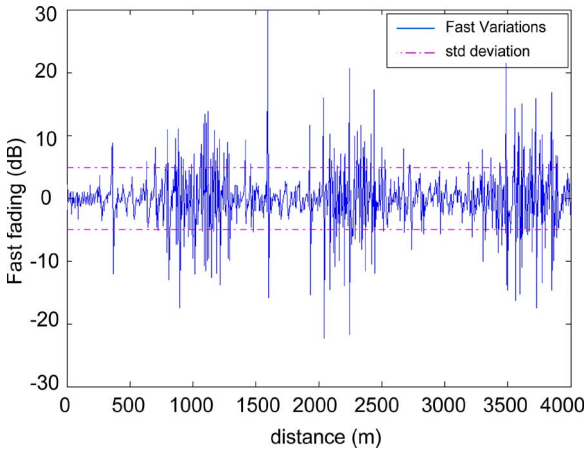

Fig. 6. Fast fading variations with multifrequency transmitters inside the tunnel. Standard deviation is $\sigma = 4.9$ dB.

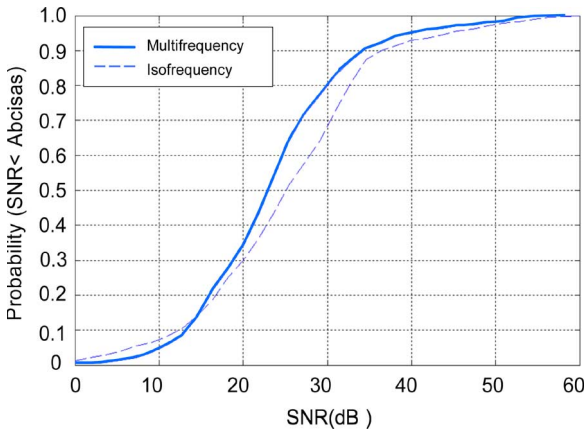

Fig. 7. Comparison of SNR for isofrequency transmitters and multifrequency transmitters.

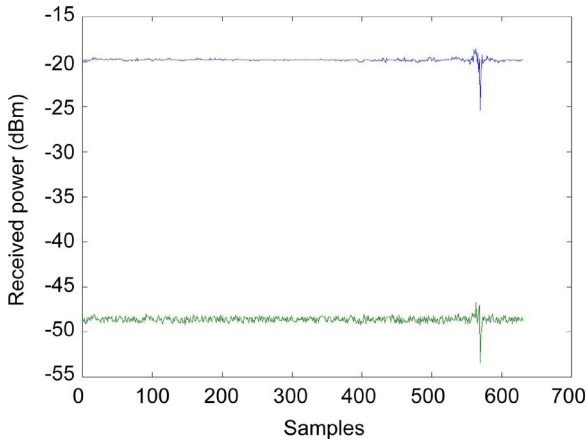

Fig. 8. Influence of two trains passing. Multifrequency transmitters. One train stopped close to one transmitter inside the tunnel.

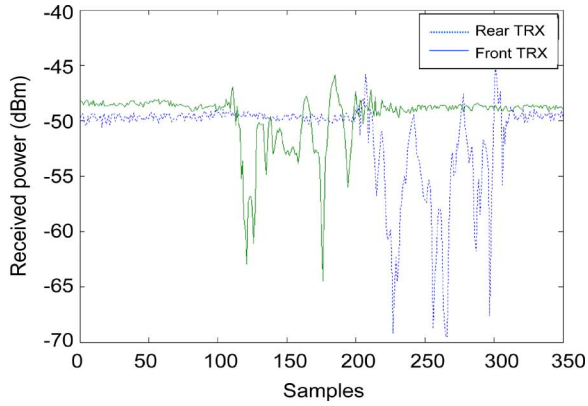

Fig. 9. Influence of two trains passing. Multifrequency transmitters. One train stopped in the center between two transmitters inside the tunnel.

standard deviation of $\sigma = 4.0$ dB as result of moderate reduction of the fast variations in the center point between two transmitters. To quantify the real quality improvement, we have compared the cumulative signal-to-noise ratio (SNR) for both cases in Fig. 7. We can see that there is a typical improvement of 2.5 dB for isofrequency transmitters. Similar results have been reported [13], [14] in measurements in subway tunnels with antennas. This result is important for the quality of service of the network because it improves signal level at the worst point of the coverage, which is the central point between two transmitters.

The second group of measurements was oriented toward evaluating the signal shadowing resulting from the blocking effect of two trains passing inside the tunnel. The problematic situation could be that a train stopped inside the tunnel could block the communications of other trains. To evaluate this situation, two trains were used, where one was stopped at different points in the tunnel on track 1, and the other runs through the tunnel on track 2. The results of these measurements are shown in Figs. 8 and 9.

In the first case, two transmitters with different frequencies, which were separated 1300 m inside the tunnel, were used. The train with the measuring equipment was stopped close to one of the transmitters on track 1, and other train went through the tunnel on track 2. The detailed result in Fig. 8 shows that the shadowing effects are reduced considerably in this situation. When the moving train passes the stationary train, we can appreciate a fade in the signal level that was received from both transmitters.

The second case was a train stopped in the middle, between two transmitters. In this case, as shown in Fig. 9, we can appreciate a moderate shadowing of up to 20 dB while the moving train passed the fixed train. The moving train first blocks the front transmitter, and when it passes the stationary train, it blocks the rear transmitter. This shadowing has a length of 200 m front and rear of the stationary train and could have some impact on the communications if the crossing point corresponds to a handover point in between two cells or if the signal margin is very limited inside the tunnel. The phenomenon is reduced when isofrequency transmitters are used. As we can see in Fig. 10, the signal received by the fixed train changes by ± 5 dB, whereas the moving train passes close to it. This signal is the power sum of the signal of the front transmitter and rear transmitter and, when the second train approaches, gives rise to multiple diffraction and reflection phenomena producing fast fading. The received signal is alternatively blocked and reflected by the moving train. Using coherent transmitters, the signal received by the fixed train changes by ± 5 dB. Therefore, there is a significant improvement as compared with

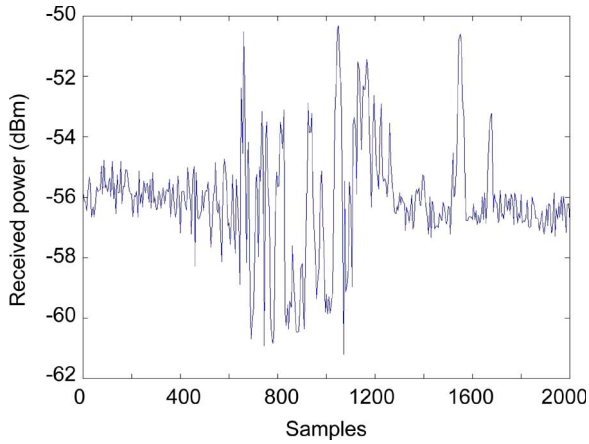

Fig. 10. Influence of two trains passing. Isofrequency transmitters. One train stopped in the center between two transmitters inside the tunnel.

multifrequency transmitters, where the moving train produces up to 20-dB fades.

III. Propagation Model

The radio planning of the different tunnels of the new high-speed railway lines requires an accurate propagation model to be able to use it on the ground, combining measurements with simulations, in a railway environment where the taking of measurements is complex and expensive. The required calculations are principally oriented toward predicting the number of repeaters needed and their location inside and outside the tunnel for a specification of signal level, tunnel geometry, curves, and fading margins. Basically, two techniques can be used to calculate the propagation inside a tunnel: 1) modal analysis and 2) ray-optical modeling. Both techniques have been widely used for tunnel propagation analysis and are well described in the literature. Modal analysis has been widely applied to the aforementioned path loss in tunnels [11]–[18], and ray-optical tracing has been described in [19]–[21], wherein it has been applied to tunnels and indoor propagation. We have combined both methods to calculate the propagation inside the tunnels. Modal analysis is used in straight tunnels, and ray tracing is used only to calculate extra attenuation in curves and in the entrance and exit of the tunnel. Correction factors are applied to compute losses by roughness and wall tilt. In the following section, we describe the bases of the model that is used, and a comparison of results with measurements is presented.

If we consider the tunnel as a waveguide, only the propagation of modes with frequencies higher than the tunnel's cutoff frequency is possible. Due to the size of the tunnels, the cutoff frequency of the fundamental modes is very low (i.e., some megahertz); therefore, at high frequencies, we find a wide range of E_{mn} hybrid modes propagating inside the tunnel for a rectangular waveguide-based model of the tunnel. Using modal theory, we can quantify the losses of horizontally and vertically polarized E_{mn} modes applying modal analysis.

Nowadays, many tunnels have a circular section, but considering that propagation losses are similar in rectangular and circular waveguides and establishing the appropriate correction coefficient, the propagation in circular tunnels can be approximated by a rectangular waveguide that is inscribed in a tunnel of radius R. The size of the rectangular waveguide that is used in the model can be computed by taking the main horizontal dimension a close to the tunnel's floor size and computing the vertical dimension b using the "rule of thumb," i.e.,

$$b = \sqrt{4R^2 - a^2}. \tag{1}$$

This equation gives good results when the tunnel's shape is greater than a semicircle, in the range $1.4R < a < 1.8R$, which is common in modern road and railway tunnels. This idealized geometry has been described [9], and deviations can be corrected by including a wall "tilt" factor in the model, as described in [11]. Finally, the model is completed, including attenuation resulting from roughness and tilt of the walls, curves, and antenna coupling factor to model the variation of antenna gain in the near-field region; therefore, the overall propagation attenuation at a distance z is computed as

$$L(z) = L(m,n)^{v/h}(z) + L_{\text{roughness}}(z) + L_{\text{tilt}}(z) + L_{\text{curv}}(z') + L_{\text{ant}} \tag{2}$$

and the calculation of these coefficients is described in Section III-B.

TABLE I
Mode Losses up to the Order $(3,3)$

F=900 MHz; a=10 m, b=5 m; ε_{r1} =ε_{r2} =5			
Mode		$\alpha(m,n)^v$	$\alpha(m,n)^h$
m	**n**	(dB/Km)	(dB/Km)
1	1	3,07	9,7
2	1	6,6	10,4
1	2	8,75	38
2	2	12,3	38,8
3	1	12,5	11,6
1	3	18,2	85,4
2	3	21,8	86
3	2	18,2	40
3	3	27,7	87,2

A. Near-Field and Far-Field Regions

If we compute the propagation losses inside the tunnel of the first (m,n) modes for vertical and horizontal polarizations (see Table I), we can clearly distinguish two regions, namely near-field and far-field regions.

In the near-field region, the field amplitude suffers strong fading and rapid decreases resulting from the contribution of many rays propagating from different grazing angles with high losses. We can also define a far-field region, where the attenuation factor is smaller because we can assume that there is only one mode propagating throughout the tunnel, namely the E_{11}^h. If we compute the attenuation of the first propagation modes (Table I), we can consider the point as the separation of both regions where E_{22}^h (horizontally polarized E-field) and E_{22}^v (vertically polarized E-field) have been strongly attenuated and higher modes have disappeared (they have greater losses). We are going to use the ray-tracing theory to compute the separation of the two propagation zones, and then, we will

apply modal analysis to compute the propagation attenuation in both regions.

E^h_{mn} and E^ν_{mn} modes are defined by the following phase relation:

$$\sin(\phi_1) = \frac{m\lambda}{2a}, \qquad m = 1, 2, 3, \ldots \tag{3}$$

$$\sin(\phi_2) = \frac{n\lambda}{2b}, \qquad n = 1, 2, 3, \ldots \tag{4}$$

where ϕ_1 and ϕ_2 are the grazing angles of incidence of the rays with the vertical and horizontal walls, respectively, and a and b are the horizontal and vertical dimensions of the tunnel, respectively. We can assume that the wavelength λ is small in comparison with a and b and approximate the sine by its argument. This is sensible at the frequencies that are studied. For instance, at 900 MHz, $\lambda = 33$ cm, and the typical values for tunnel dimensions are of several meters. Thus

$$\phi_1 = \frac{m\lambda}{2a}, \qquad n = 1, 2, 3, \ldots \tag{5}$$

$$\phi_2 \approx \frac{zn\lambda}{2b}, \qquad n = 1, 2, 3, \ldots. \tag{6}$$

The attenuation depends on the number of reflections of the rays, i.e., N_1 and N_2, and the reflection coefficient of the signal over the vertical and horizontal walls along a distance z. The number of reflections is easily obtained from (5) and (6). Thus

$$N_1 \approx \frac{zm\lambda}{2a^2} \tag{7}$$

$$N_2 \approx \frac{zn\lambda}{2b^2}. \tag{8}$$

With these numbers, we can define the breaking point or limit of the near-field and far-field regions as the distance where the fundamental modes E^h_{11} and E^v_{11} have suffered one reflection, considering vertical and horizontal walls. At this distance, the remaining modes have suffered several reflections and have been considerably more attenuated because of both the higher number of reflections and the lower reflection coefficient resulting from a lower incident angle.

With both $N_1 = 1$ and $N_2 = 1$ in (7) and (8), the distance from the transmitter to the "breaking point" is defined by

$$Z_{\mathrm{NF}} \approx \mathrm{Max}\left(\frac{a^2}{\lambda}, \frac{b^2}{\lambda}\right). \tag{9}$$

Z_{NF} is directly proportional to the square of the largest dimension of the tunnel and inversely proportional to the wavelength; therefore, from the transmitter to a distance Z_{NF}, we consider that there are horizontally and vertically polarized E_{mn} modes, and from Z_{NF}, we consider that only E^h_{11} mode propagates. With this consideration, we are going to define a dual-slope propagation model for propagation losses in the near field and in the far field.

B. Propagation Attenuation

The signal propagating through the tunnel is made up of several modes that propagate with different attenuations. The calculation of the overall propagation attenuation from a transmitter to a receiver can be simplified if we consider that the power of each mode that travels through the tunnel is independent of the others; therefore, we can assume that the total power is the power sum of each mode. This supposition is based on the fact that modes are approximately orthogonal. With this approximation,, we can compute the following mode loss expressions for horizontal and vertical polarizations that are applicable for each (m, n) mode:

$$\alpha(m,n)^h = 4.343\lambda^2 \left(\frac{m^2\varepsilon_{r1}}{a^3\sqrt{\varepsilon_{r1}-1}} + \frac{n^2}{b^3\sqrt{\varepsilon_{r2}-1}}\right) \text{ dB/m} \tag{10}$$

$$\alpha(m,n)^\nu = 4.343\lambda^2 \left(\frac{m^2}{a^3\sqrt{\varepsilon_{r1}-1}} + \frac{n^2\varepsilon_{r2}}{b^3\sqrt{\varepsilon_{r2}-1}}\right) \text{ dB/m} \tag{11}$$

where ε_{r1} and ε_{r2} are the relative permittivities of the vertical and horizontal walls, respectively. The bigger the tunnel section, the smaller is the attenuation that is experienced by the modes propagating throughout the tunnel, because losses are inversely proportional to the cube of the height and width of the tunnel. With this propagation constant, we can compute the propagation attenuation at a certain distance z, considering losses as the rms contribution of modes for both polarizations, i.e.,

$$L^{v/h}_{mn}(z) = 10\,\log_{10}\left[\sum_{i=1}^{m}\sum_{j=1}^{n} \times \sqrt{10^{2\alpha(i,j)^h z} + 10^{2\alpha(i,j)^\nu z}}\right] \text{dB}. \tag{12}$$

In addition to this, losses are directly proportional to the square of the order of the modes, so that higher modes experience stronger attenuation. In fact, we can consider that from a certain distance, there is no propagation of modes except for the main one, namely the E^h_{11} and E^ν_{11}. Losses are also directly proportional to the square of the wavelength.

Additional corrections to the model must be considered because of the roughness and tilt of the walls. Both factors, which were modeled by Emslie *et al.* [11] and Zhang and Hwang [17], generate diffuse radiation that reduces the power of the modes that propagate through the tunnel. This phenomenon increases the losses of all modes, but it is particularly sensitive in the far-field region, where it moderately increases the losses of the fundamental mode E^h_{11}. Roughness losses are particularly important at low frequencies and in old subway tunnels. In modern tunnels, wall roughness is usually low.

Tilt losses are more important in semicircular tunnels and must be adjusted carefully for each tunnel.

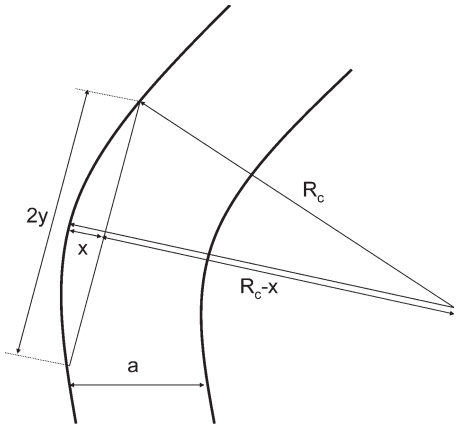

Fig. 11. Geometry used to compute the attenuation of curves.

C. Curve Attenuation

To add more accuracy to the model, we have expanded the waveguide model, including losses for tunnel curves. To compute extra losses as a result of curves, we have used the shooting and bouncing ray method. Basically, this method computes the attenuation considering the number of reflections in the vertical and horizontal walls, i.e., N_1 and N_2, and the reflection coefficients of vertical and horizontal walls, i.e., Γ_1 and Γ_2. For each ray of initial power P_o, the power P after $N_{1,2}$ reflections can be computed as

$$\frac{P}{P_o} = |\Gamma_1|^{2N_1} \cdot |\Gamma_2|^{2N_2}. \tag{13}$$

As tunnels usually only have curves on the horizontal axis, there are additional attenuations resulting from the increase in the number of reflections in the vertical walls.

To compute the number of reflections in the vertical walls, we define a curved section by using the radius of the curve R_c and the horizontal section of the tunnel a, as shown in Fig. 11. The distance between the external wall of the tunnel and the ray that is launched along the tunnel width is x. The value of y is defined by

$$y = \sqrt{R_c^2 - (R_c - x)^2}. \tag{14}$$

If at each distance $2y$ the ray suffers a reflection in the vertical walls of the tunnel, the number of reflections per meter is inversely proportional to the distance $2y$, i.e.,

$$N_{1c} \propto \frac{1}{2y} = \frac{1}{2\sqrt{R_c^2 - (R_c - x)^2}}. \tag{15}$$

Now, we define ϕ_1 as the grazing angle of incidence of the rays with the vertical walls, as we have done in (3) and (5) to compute the near-field region, but now, we consider a curved tunnel. Thus, we have

$$\phi_1 = \tan^{-1}\left(\frac{\sqrt{R_c^2 - (R_c - x)^2}}{R_c - x}\right). \tag{16}$$

The attenuation of an electromagnetic wave (ray) inside the tunnel as a result of the curvature is computed as the average of the losses that are suffered by all the rays that are launched along the tunnel width a, at a certain distance z'. Therefore, the attenuation that is suffered by a ray depends on the length of the curve, the reflection coefficient, and the roughness of the walls. Considering these parameters, the extra attenuation resulting from a curve of length z' can be computed as

$$L_{\text{curv}}(z') = 10\,\log_{10}\left\lfloor(\rho|\Gamma|)^{2zN_{1c}}\right\rfloor \tag{17}$$

where ρ is the coefficient that considers the roughness of the walls, i.e.,

$$\rho = \exp\left(-2\left(\frac{2\pi h \sin(\phi_1)}{\lambda}\right)^2\right) \tag{18}$$

where ϕ_1 is the angle of incidence with respect to the reflection surface, and h is the average square roughness of the walls.

The reflection coefficient of each ray Γ is computed using Fresnel's formulas, and its value depends on the polarization. For vertical polarization, we must use

$$\Gamma = \Gamma_\nu = \frac{\varepsilon_{r1}^* \text{sen}(\phi_1) - \sqrt{\text{sen}^2\phi_1 + \varepsilon_{r1}^* - 1}}{\varepsilon_{r1}^* \text{sen}(\phi_1) + \sqrt{\text{sen}^2\phi_1 + \varepsilon_{r1}^* - 1}} \tag{19}$$

whereas for horizontal polarization, we must use

$$\Gamma = \Gamma_h = \frac{\text{sen}(\phi_1) - \sqrt{\text{sen}^2\phi_1 + \varepsilon_{r1}^* - 1}}{\text{sen}(\phi_1) + \sqrt{\text{sen}^2\phi_1 + \varepsilon_{r1}^* - 1}}. \tag{20}$$

In (19) and (20), the permittivity is a complex number that is made up of the dielectric constant and the conductivity of the tunnel walls, i.e.,

$$\varepsilon_{r1}^* = \varepsilon_{r1} - j\frac{\sigma}{w\varepsilon_0}. \tag{21}$$

In modern concrete tunnels, we can consider the conductivity of the walls as low; therefore, the effect on the reflection coefficient is negligible, and the permittivity can be considered as real. For example, at 900 MHz, with the typical values for concrete $\varepsilon_{r1} = 5$ and $\sigma = 10^{-3}$ S/m, $\varepsilon_{r1}^* = 5 + 0.02j$; therefore, it can be considered that $\varepsilon_{r1}^* \approx \varepsilon_{r1}$.

All of these expressions have been defined for vertical surfaces, and they are also applicable to horizontal surfaces. With these equations, we can compute the attenuation of a curve of length z'. First, we apply modal analysis to compute the propagation attenuation along all the tunnels, and then, on the curved zones, we increase the propagation losses using the aforementioned ray-tracing technique.

D. Overall Propagation Attenuation

Considering the basic mode losses and roughness, tilt, and the curve coefficients that were defined, we can predict propagation losses with the distance using two different approaches, one for the near-field region and the other for the far-field region. The separation of both regions is defined by the

TABLE II
DATA APPLIED IN THE SIMULATION OF THE PROPAGATION IN THE TUNNEL

Test Transmitter outside the tunnel	
Distance (from the extreme of the tunnel)	2,200 m
Antenna height	20 m
Environment	Rural
Isotropic radiated power	46.8 dBm
Test transmitters inside tunnel	
First transmitter	1,000 m
Second Transmitter	2,300 m
Third Transmitter	3,500 m
Isotropic radiated power	43.3 dBm
Others	
Receiver antenna gain	2.15 dB
Frequency	900 MHz
Characteristics of the tunnel	
Roughness (m)	0.12 m
ε_{r1} (vertical walls)	5
ε_{r2} (horizontal walls)	5
Tilt angle	0.25º
Height "b"(m)	5.4 m
Width "a" (m)	10.7 m
Length "z" (m)	4,000 m
Characteristics of the curve	
Number of curves	1
Radius	3,500 m
Starting point	1,200 m
Final point	2,800 m

breaking point Z_{NF}, as computed in (9). The following expressions provide a way of calculating the losses in decibels.

In the near-field region, $z < Z_{\mathrm{NF}}$, we consider losses of (m, n) modes as the rms contribution of modes up to (10, 10) for both polarizations, i.e.,

$$L(z) = L_{\mathrm{ant}} + L_{mn}^{v/h}(z) + L_{\mathrm{roughness}}(z) + L_{\mathrm{tilt}}(z) + L_{\mathrm{curv}}(z'). \quad (22)$$

In the far-field region, $z > Z_{\mathrm{NF}}$, we only consider losses at the first-order (1, 1) vertical or horizontal mode, i.e.,

$$L(z) = L_{\mathrm{ant}} + L_{11}^{v/h}(z) + L_{\mathrm{roughness}}(z) + L_{\mathrm{tilt}}(z) + L_{\mathrm{curv}}(z'). \quad (23)$$

In both cases, it is also necessary to add a constant attenuation factor between antennas, which is called the "antenna coupling loss" L_{ant}. This factor depends on the near-field characteristics of the antennas and can be easily measured in the laboratory or computed, as defined in [18].

IV. SIMULATION RESULTS

To validate the proposed model, simulations have been compared with the previously described measurements. The input data for the simulations are the tunnel and transmitter parameters, as detailed in Table II.

With these data, the propagation model has been applied in the entire tunnel considering up to $(m = 10,\ n = 10)$ rays. Extra attenuation in the curves has been computed using ray tracing.

The antenna coupling factor has been measured in the laboratory in an anechoic chamber with the transmitting and receiving antennas that were used in the measurements. Return losses at the entrance and exit of the tunnel has been computed using the model that is described in [20]. Propagation losses outside the tunnel have been computed using free-space losses because there was line of sight between the tunnel entrance and the external base station. The different contributions to the propagation losses are summarized in Table III.

TABLE III
COMPUTED LOSSES AND ATTENUATION COEFFICIENTS

Losses inside the tunnel (dB/Km)	
Tilt losses (θ=0.2º)	9.87
Roughness losses (0.12 m)	0.8
$E_{11}{}^{H}$ losses	2.65
Curve losses (dB/Km)	
Average Ray tracing curve losses	4.33
Additional factors	
Return losses at the entrance/ exit of the tunnel	20 dB
Near-field/far-field braking point	347 m
Antenna coupling factor (transmitter-receiver)	57 dB

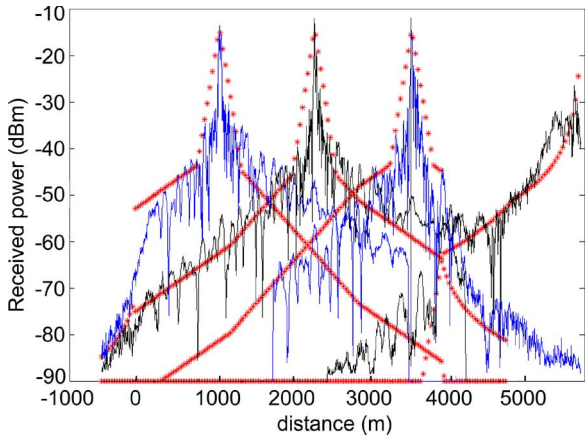

Fig. 12. Comparison of measurements and modeling. Multifrequency transmitters.

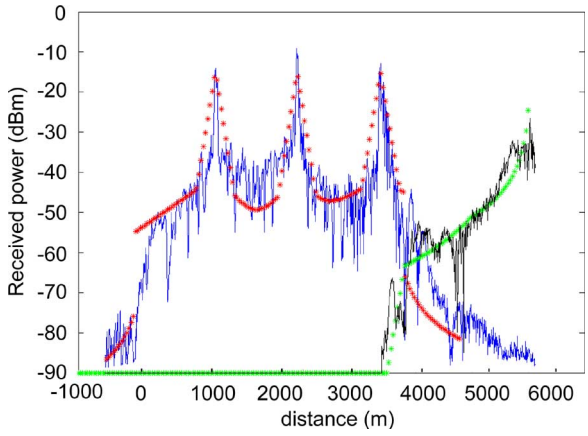

Fig. 13. Comparison of measurements and modeling. Isofrequency transmitters.

Comparisons with measurements are shown in Fig. 12 for multifrequency transmitters and in Fig. 13 for isofrequency transmitters. In these figures, we can see that the modal theory gives good approximation to predict the losses throughout the tunnel. We can see that the model is more accurate in the

far-field region than in the near-field region. This is because in the near-field region, which is in the first 347 m in our tunnel, there are a lot of modes propagating at the same time, and the overall losses are much more variable than in the far-field region, where most modes have been extinguished. In this region, we only consider the dominant modes with (m, n) up to the order of ten, and the model gives a total attenuation of 13.31 dB/km in the straight part of the tunnel.

These extra losses have been computed with ray tracing and give a factor of 4.33 dB for the parameters of the tunnel and curve, as given in Table II. This coefficient is added as an increase in the losses throughout the entire length of the curve, and as we can see in Figs. 12 and 13, the results show good agreement with the measurements.

We can conclude that the model is easy to apply and accurate enough to predict losses in a tunnel and to determine the number of transmitters, power, antenna gain, and location to obtain good coverage for a specific signal power level inside and outside the tunnel.

In the curved area, it is necessary to add the extra losses.

V. Conclusion

A complete measurement and modeling of a long railway tunnel has been reported. Measurements have demonstrated the good propagation characteristics of the railway tunnels and the viability of using distributed antennas inside, even if a high signal level is specified.

We have verified how, in a straight tunnel, the signal from a transmitter propagates in the multimode for the first 300 m with strong losses, and after the first 100 m, only the TE_{11} mode survives, and therefore, propagation loss is much lower.

Another important aspect is the strong fade when the train passes from inside to outside the tunnel due to wave impedance change and diffraction effects. In our measurements, a 20-dB loss was measured. This loss must be taken into account when feeding a tunnel with external antenna or when there are several tunnels with a gap of open track between them.

Other interesting results are the improvements achieved using simultaneous transmission using frequency coherent transmitters. With this solution, fast fading is reduced, thus improving average signal to noise of 2.5 dB. This improvement is equivalent to the use of spatial diversity in open areas.

Fading resulting from passing inside the tunnels is another important result for the planning of the network. Measurements suggest that a 15- to 20-dB margin must be considered to mitigate losses resulting from a train passing inside the tunnels in multifrequency operation. This margin can be reduced to 3–5 dB using isofrequency repeaters, as it has been demonstrated with the measurements that were taken.

Finally, a complete propagation model for railway applications has been proposed. The model has combined the use of modal analysis in straight zones with the use of ray tracing to calculate extra attenuation in curves at the entrance/exit of the tunnel. A complete table with correction factors has been given and verified with measurements.

The model is easy to use, fast, and accurate enough for radio planning in a railway environment. It has been successfully used in the radio planning of 40 km of tunnels of the new Spanish Madrid–Lleida high-speed line, and it has been very useful in predicting the location, number of repeaters, handover point, and signal margins that are required for the coverage of a specific tunnel with antennas.

References

[1] ERRI Committee A 175, *Railway Radio Propagation Including Aspects of Transmission of Safety Information*. ERRI A 175/RP2, Utrecht, The Netherlands, 7/1992.

[2] M. V. S. N. Prasad and R. Singh, "Terrestrial mobile communications train measurements in Western India," *IEEE Trans. Veh. Technol.*, vol. 52, no. 3, pp. 671–682, May 2003.

[3] N. Monk and H. S. Winbigler, "Communication with moving trains in tunnels," *IRE Trans. Veh. Commun.*, vol. PGVC-7, no. 1, pp. 21–28, Dec. 1956.

[4] Y. P. Zhang, "Practical performance of digital cellular system in mass rapid transit environments," *Int. J. Commun. Syst.*, vol. 18, pp. 143–157, Dec. 2004.

[5] [Online]. Available: http://www.uic.asso.fr

[6] C. Briso-Rodríguez, C. Cortes, F. J. Arques, and I. Alonso, "Requirements of GSM technology for the control of high speed trains," in *Proc. Pers., Indoor, Mobile Radio Commun. Conf.*, Feb. 2002, pp. 792–793.

[7] D. Didascalou, J. Maüer, and W. Wiesbeck, "Subway tunnel guided electromagnetic wave propagation at mobile communications frequencies," *IEEE Trans. Antennas Propag.*, vol. 49, no. 11, pp. 1590–1596, Nov. 2001.

[8] M. Lienard and P. Degauque, "Propagation in wide tunnels at 2 GHz: A statistical analysis," *IEEE Trans. Veh. Technol.*, vol. 47, no. 4, pp. 1322–1328, Nov. 1998.

[9] P. Mariage, M. Lienard, and P. Degauque, "Theoretical and experimental approach of the propagation of high frequency waves in road tunnels," *IEEE Trans. Antennas Propag.*, vol. 42, no. 1, pp. 75–81, Jan. 1994.

[10] Y. P. Zhang, Z. R. Jiang, T. S. Ng, and J. H. Sheng, "Measurements of the propagation of UHF radio waves on an underground railway train," *IEEE Trans. Veh. Technol.*, vol. 49, no. 4, pp. 1342–1347, Jul. 2000.

[11] A. G. Emslie, R. L. Lagace, and P. F. Strong, "Theory of the propagation of UHF radio waves in coal mine tunnels," *IEEE Trans. Antennas Propag.*, vol. AP-23, no. 2, pp. 192–205, Mar. 1975.

[12] S. H. Chen and S. K. Jeng, "SBR image approach for radio wave propagation in tunnels with and without traffic," *IEEE Trans. Veh. Technol.*, vol. 45, no. 3, pp. 570–578, Aug. 1996.

[13] A. Coraiola and B. Sturani, "Using a pair of phased antennas to improve UHF reception/transmission in tunnels," *IEEE Antennas Propag. Mag.*, vol. 42, no. 5, pp. 40–47, Oct. 2000.

[14] R. J. Jakubowski, "Results of distributed antenna and leaky feeder systems tests at 800 MHz in Washington D.C. metro system tunnels," in *Proc. IEEE 44th Veh. Technol. Conf.*, 1994, vol. 2, pp. 1113–1116.

[15] C. L. Holloway, D. A. Hill, R. A. Dalke, and G. A. Hufford, "Radio wave propagation characteristics in lossy circular waveguides such as tunnels, mine shafts and boreholes," *IEEE Trans. Antennas Propag.*, vol. 48, no. 9, pp. 1354–1366, Sep. 2000.

[16] Y. P. Zhang and Y. Hwang, "Theory of the radio-wave propagation in railway tunnels," *IEEE Trans. Veh. Technol.*, vol. 47, no. 3, pp. 1027–1036, Aug. 1998.

[17] Y. P. Zhang and Y. Hwang, "Enhancement of rectangular tunnel waveguide model," in *Proc. APMC*, 1997, vol. 1, pp. 197–200.

[18] Y. P. Zhang, "Novel model for propagation loss prediction in tunnels," *IEEE Trans. Veh. Technol.*, vol. 52, no. 5, pp. 1308–1314, Sep. 2003.

[19] M. Lienard and P. Degauque, "Characterization of the propagation channel in a high speed train environment," in *Proc. 9th MELECON*, May 18–20, 1998, vol. 1, pp. 260–262.

[20] F. Martí Pallarés, F. J. P. Juan, and L. Juan-Llácer, "Analysis of path loss and delay spread at 900 MHz and 2.1 GHz while entering tunnels," *IEEE Trans. Veh. Technol.*, vol. 50, no. 3, pp. 767–776, May 2001.

[21] M. Nilsson, J. Slettenmark, and C. Beckman, "Wave propagation in curved road tunnels," in *Proc. IEEE Antennas Propag. Soc. Int. Symp.*, Jun. 21–26, 1998, vol. 4, pp. 1876–1879.

[22] Y. P. Zhang and H. J. Hong, "Ray-optical modeling of simulcast radio propagation channels in tunnels," *IEEE Trans. Veh. Technol.*, vol. 53, no. 6, pp. 1800–1808, Nov. 2004.

Cesar Briso-Rodríguez was born in Valladolid, Spain. He received the Ingeniero de Telecomunicación and Ph.D. degrees from the Universidad Politécnica de Madrid, Madrid, Spain, in 1996 and 1999, respectively.

Since 1996, he has been an Assistant Professor with the Escuela Universitaria de Ingeniería Técnica de Telecomunicación, Universidad Politécnica de Madrid. He has taught courses in microwave circuit design, digital communications, and communications applied to transportation systems. His research activity has been focused in the area of design and development of high-frequency communication systems for complex environments.

Prof. Briso-Rodríguez was a recipient of an award for the best Ph.D. thesis in GSM communications from the Spanish Association of Telecommunications Engineers.

Javier M. Cruz was born in Tenerife, Spain, in 1980. He received the Ingeniero de Telecomunicacion degree from the Universidad Politécnica de Madrid, Madrid, Spain, in 2004.

From 2005 to 2006, he was with Agilent Technologies, Barcelona, Spain. Since 2006, he has been in charge of the communication systems of the metropolitan tramway from Tenerife. His research interests are focused on the propagation modeling and instrumentation equipment applied to high-frequency communications.

Jose I. Alonso (M'90) was born in Villacañas, Toledo, Spain. He received the Ingeniero de Telecomunicación and Ph.D. degrees from the Universidad Politécnica de Madrid, Madrid, Spain, in 1982 and 1989, respectively.

From 1982 to 1985, he was a Microwave Design Engineer with Telettra Spains S.A. (now Alcatel Standard S.A.). In 1985, he joined the Departamento de Señales, Sistemas y Radiocomunicaciones, Escuela Técnica Superior de Ingenieros de Telecomunicación, Universidad Politécnica de Madrid, where he is currently a Full Professor. He has taught courses in microwave circuit design, electrical networks and filter theory, test and measurements of microwave circuits, and laboratories related to analog and digital communication systems. He has been with the Grupo de Microondas y Radar, where he works on research in the areas of the analysis and simulation of high-speed/high-frequency integrated circuits (MMIC) and their interconnections. He is also involved in the development of circuits and systems for local multipoint distribution systems and wireless local-area networks.